



PET imaging of TREM2 in amyloid-beta induced neuroinflammation

Amelia D Dahlén¹ · Sahar Roshanbin¹ · Ximena Aguilar¹ · Nadja M Bucher¹ · Sara Lopes van den Broek¹ · Dag Sehlin¹ · Stina Syvänen¹

Received: 5 February 2025 / Accepted: 14 May 2025 / Published online: 28 May 2025
© The Author(s) 2025

Abstract

Purpose The triggering receptor expressed on myeloid cells 2 (TREM2) has become a promising target for biologics in both monitoring and treating neuroinflammation in Alzheimer’s disease (AD). This study aimed to develop and compare bispecific anti-TREM2 antibodies featuring different transferrin receptor (TfR) binders to enhance brain delivery, identifying the most suitable format for in vivo PET imaging of TREM2 in transgenic AD mice.

Methods Three bispecific TREM2-antibody formats were produced and evaluated for their ability to cross the blood-brain barrier (BBB) via TfR-mediated transcytosis and bind TREM2. Blood concentration profiles up to 72 h post-injection (p.i.), and ex vivo brain uptake of iodine-125-labeled antibody constructs were quantified in App^{NL-G-F} and age-matched wild type (WT) mice using a γ -counter. The best-performing bispecific TREM2-antibody was radiolabeled with iodine-124 and used for in vivo PET imaging of brain TREM2 levels in App^{NL-G-F} mice at 72 h p.i. Brain TREM2 concentrations were subsequently quantified using ELISA.

Results The antibody format carrying two scFv8D3 TfR-binders (IgG-scFv₂), demonstrated the highest brain concentrations of all tested bispecific constructs. This antibody also exhibited significantly higher brain concentrations in App^{NL-G-F} mice compared to WT mice at both 48 and 72 h p.i. This difference was further visualized and quantified through in vivo PET imaging. Moreover, brain concentrations of the antibody ligand correlated with elevated TREM2 levels in brain homogenates.

Conclusion These findings highlight IgG-scFv₂ as a promising radioligand for in vivo PET imaging of TREM2, advancing non-invasive neuroinflammation studies and supporting drug development for AD and other neurodegenerative diseases.

Keywords Neuroinflammation · Antibody-based PET · Alzheimer’s disease · Bispecific antibody · The blood-brain barrier

Introduction

In the short time span of twelve months, two antibody-based treatments for Alzheimer’s disease (AD) have been approved by the Food and Drug Administration (FDA). Lecanemab by Eisai/BioArctic and Donanemab by Eli Lilly have both been successful in slowing cognitive decline and the removal of neuropathological amyloid-beta (A β) protein in the AD brain [1, 2]. These results build on the progress of continually evolving AD biomarkers, with positron emission tomography (PET) imaging being particularly notable.

The use of amyloid radioligands to monitor the reduction of brain A β during immunotherapy has advanced AD research, opening up for new treatment possibilities that go beyond purely symptomatic interventions.

With this said, AD is a multifaceted disease likely requiring multiple lines of treatment to combat the neurodegenerative processes. Alongside the toxic species of A β and neurofibrillary tau tangles, neuroinflammation is now a widely recognized component of AD [3]. The accumulation of A β may initiate neuroinflammatory cascades of cytokines and chemokines, mediated by microglia and astrocytes of the central nervous system (CNS), which contribute to the disease severity [4]. Thus, neuroinflammation in AD calls for its own treatment approach. Capturing neuroinflammation through in vivo imaging, e.g. PET radioligands, could therefore carry great diagnostic potential for AD patients and for the development of new anti-inflammatory drugs.

✉ Stina Syvänen
stina.syvanen@uu.se

¹ Department of Public Health and Caring Sciences, Section of Molecular Geriatrics, Uppsala University, Uppsala, Sweden

Mitochondrial 18-kDa translocator protein (TSPO) is the most commonly investigated target for PET imaging of neuroinflammation, and has been visualized using [^{11}C]PK11195, [^{18}F]DPA-714, [^{11}C]PBR28 and [^{18}F]GE-180 among others [5–8]. However, interpretation of TSPO PET imaging is confounded by large inter-individual variability in binding affinity due to the genetic polymorphism rs6971 [7, 9]. Less polymorphism sensitive radioligands, such as [^{18}F]BS224, have been gaining traction as third generation TSPO-tracers [10]. Nevertheless, the interpretation of TSPO PET is hampered by TSPO being expressed in both microglia and astrocytes in AD and non-AD brains [11].

Another neuroinflammation target is monoamine oxidase B (MAO-B), which metabolizes dopamine and histamine in the brain [12]. It is localized in the mitochondrial membrane of astrocytes and is targeted by radioligands such as [^{11}C]DED [13]. Upon its covalent binding to MAO-B, [^{11}C]DED irreversibly inhibits MAO-B's enzymatic actions and is therefore referred to as a suicide enzyme inactivator [13]. PET-imaging with [^{11}C]DED captures elevated MAO-B in early disease stages, but does not reflect astrogliosis as the A β burden grows [14, 15]. Instead, the PET-ligand [^{11}C]BU99008 that binds to the Imidazoline 2 Binding Site (I2BS) on the astrocytic mitochondrial membrane may be better at capturing the later stages of astrogliosis [16]. For example, [^3H]BU99008 shows higher post mortem binding in brain sections from sporadic AD cases in comparison to control cases [17]. Still, the heterogeneity of both microglia and astrocytes throughout the disease progression makes it difficult to follow the neuroinflammatory trajectory. Thus, there is an unmet need for new improved and specific PET radioligands for the visualization of neuroinflammation.

Triggering receptor expressed on myeloid cells 2 (TREM2) is expressed by microglia and regulates the inflammatory response by dampening the secretion of pro-inflammatory cytokines and improving microglial phagocytosis of A β [18, 19]. Several point mutations in the *TREM2* gene have been linked to AD: the most notable amino acid substitution, R47H, leads to a four-fold increased risk of developing late-onset AD [20, 21]. Sporadic AD patients carrying TREM2 risk variants have a higher percentage of dystrophic microglia, a phenomenon recapitulated in pre-clinical studies where TREM2 deficiency leads to microglial accumulation of ApoE and impaired microgliosis [22, 23]. Upon binding of TREM2's ligands, such as A β and apolipoprotein E (ApoE), to the extracellular domain, the intracellular adapter protein DNAX-activation protein 10 or 12 (DAP10/12) binds to the cytoplasmic tail of TREM2 to initiate downstream signaling [18]. The extracellular domain of TREM2 can initiate parallel inflammatory pathways following cleavage by a disintegrin and metalloproteinase domain-containing protein (ADAM10 and 17) at

histidine 157 and serine 158, resulting in soluble TREM2 (sTREM2) [24]. Although the functions of sTREM2 are not fully delineated, it may negatively impact the anti-inflammatory processes prompted by TREM2 activation, as fewer ligands can bind to the ectodomain [25].

With growing interest in developing therapeutics to mitigate neuroinflammation in AD, antibody-based PET radioligands targeting TREM2 present a promising alternative to the aforementioned small-molecule radioligands for visualizing activated microglia. However, to use antibodies as brain PET radioligands, their inherently low brain delivery across the blood-brain barrier (BBB) has to be increased. This can be achieved by engineering antibodies into bispecific formats to also target the transferrin receptor 1 (TfR1, hereafter TfR) expressed at the BBB. Thus, TfR acts as a shuttle for the antibody and can increase antibody brain concentrations by 10- to 80-fold, depending on the dose and the bispecific format used [26–30]. We have previously demonstrated that such bispecific antibodies, after radiolabeling, can serve as PET radioligands to detect proteins like A β and alpha-synuclein in the living brain [31–37]. Prior preclinical TREM2 antibody-based neuroimaging studies have used [^{124}I]-labeled AF1729 in tg-ArcSwe mice and [^{64}Cu]-labeled 4D9 in 5xFAD mice [38, 39]. The antibody-based radioligands described in this study are based on the antibody 14D3 [40], which binds the N-terminal of TREM2 and inhibits the cleavage of sTREM2.

The aim of this study was to explore and compare bispecific formats of the anti-TREM2 antibody, with the ultimate goal of developing a PET ligand for in vivo visualization and quantification of TREM2. This work contributes to advancing PET imaging tools for studying neuroinflammatory markers in neurodegenerative diseases.

Materials and methods

Antibody design

The antibodies were designed based on the amino acid sequence of the variable domains of monoclonal antibody 14D3 (Fig. 1), which binds between amino acids 148–166 of murine membrane bound TREM2 and between amino acids 148–166 of human membrane bound TREM2 [40]. Monospecific TREM2 antibodies, IgG^{wt} (RmAb14D3, 148 kDa) and IgG (RmAb14D3_{LALA-PG}, 148 kDa), had murine IgG2c backbones suitable for B16 mouse lines (Fig. 1a, c). IgG^{wt}-scFv₂ (RmAb14D3-scFv8D3, 203 kDa) and IgG-scFv₂ (RmAb14D3_{LALA-PG}-scFv8D3, 203 kDa) contained bivalent single-chain variable fragments (scFv) of the TfR binding antibody 8D3 fused to the c-termini of the light chains [27, 41] (Fig. 1b, d). The monovalent knob-in-hole

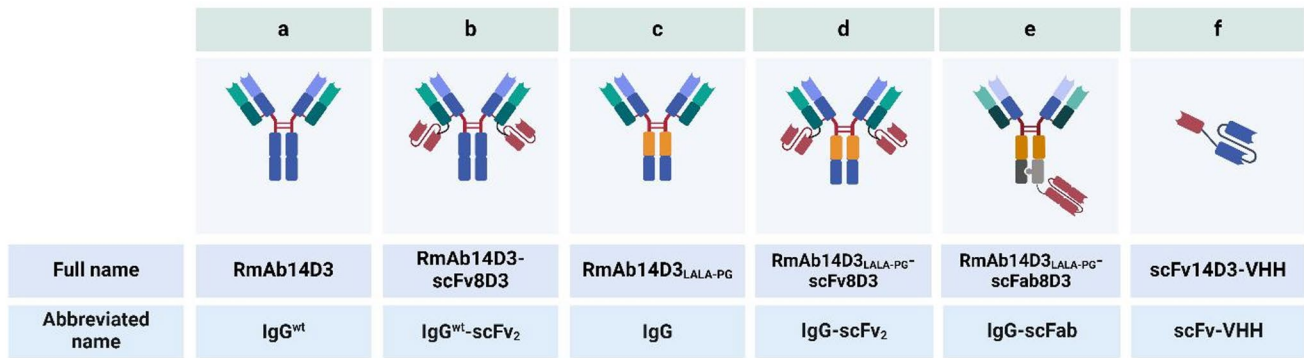


Fig. 1 Produced anti-TREM2-anti-TfR constructs

antibody IgG-scFab (RmAb14D3_{LALA-PG}-scFab8D3, 206 kDa) contained a single-chain Fab fragment (scFab) of 8D3 attached to the c-terminus of the heavy chain [28, 30] (Fig. 1e). The smallest scFv-VHH (scFv14D3-VHH, 41 kDa), consisted of a TfR Nanobody of camelid origin coupled via a linker to scFv14D3 [42] (Fig. 1f). IgG, IgG-scFv₂ and IgG-scFab contained the LALA-PG mutations, which eliminate Fcγ receptor binding to reduce antibody-dependent cellular cytotoxicity [43] (Fig. 1c-e). For antibody production and purification protocols, please see [Supplementary Information](#).

Enzyme-linked immunosorbent assays (ELISA)

To assess the post-production binding affinity of the antibodies to murine TfR protein and murine TREM2 protein, indirect ELISAs were performed in half-area 96-well plates (Corning inc.). The plate was coated with the following proteins diluted in phosphate buffered saline (PBS): murine TfR protein (0.5 μg/mL, in-house produced), murine TREM2 protein (5 μg/mL, SinoBiological, 158–50149-M02H-100) and human TREM2 protein (0.5 μg/mL, SinoBiological, 158–11084-H08H-100). Plates were incubated overnight at 4 °C. Following incubation, the plates were blocked with 1% bovine serum albumin (BSA) for 2 h at RT on a shaker. Biotinylated bispecific antibodies were added in 5x dilution series, starting at 250 nM in ELISA incubation buffer (PBS with 0.1% BSA, 0.05% Tween, and 0.15% Proclin), and incubated overnight at 4 °C. Horseradish peroxidase (HRP) conjugated streptavidin (Mabtech, 3310-9-1000) was then added at a 1:2000 dilution for 1 h at RT, on a shaker.

To compare binding affinity before and after radiolabeling, the plate was coated with the following proteins and antibodies, diluted in PBS: anti-mouse IgG (0.5 μg/mL, VECTOR, AI-2000-1.5), anti-human IgG (0.5 μg/mL, Mabtech, MT91/145), StrepMAB-Classic (0.5 μg/mL, Iba Life Sciences, 2–1507-001), murine TfR protein (0.5 μg/mL, in-house produced), and murine TREM2 protein (5 μg/mL, SinoBiological, 158–50149-M02H-100).

Antibodies were added in 5x dilution series, starting at 50 nM in ELISA incubation buffer, and incubated overnight at 4 °C. Detection antibodies, including anti-mouse-F(ab')₂-HRP (Jackson ImmunoResearch Laboratories, 115-035-006), anti-human-F(ab')₂-HRP (Jackson ImmunoResearch Laboratories, 109-036-006), StrepMAB-Classic HRP (Iba Lifesciences, 2–1509-001) or Anti-Camelid VHH Antibody [HRP] (MonoRab™, A01861) were added at a 1:2000 dilution for 1 h at RT, on a shaker.

K blue aqueous TMB substrate (Neogen Corp., Lexington, USA) was used to develop ELISA signals and the reaction was stopped with 1 M H₂SO₄. The plates were read with a spectrophotometer at 450 nm.

Animals

Knock-in App^{NL-G-F} mice [44], expressing human APP with the Swedish (KM670/671 NL), Arctic (E693G) and Beyreuter/Iberian (I716 F) mutations and wild-type (WT) mice (C57BL/6 JBomTac) were used for in vivo ($n = 8$) and ex vivo ($n = 99$) studies (Supplementary Table S1). Young mice (4–5 months) were used in the initial brain uptake studies and aged mice (11.5–19 months) were used in subsequent brain retention studies. Both male and female animals were included (Supplementary Table S1). App^{NL-G-F} male mice weighed 40.1 ± 4.2 g, App^{NL-G-F} female mice 29.9 ± 4.7 g, WT male mice 36.9 ± 4.8 g and WT female mice 29.7 ± 5.0 g. The animals were housed in an approved animal facility at Uppsala University with *ad libitum* access to food and water. The study adhered to the Animal Research: Reporting of In Vivo Experiments (ARRIVE) guidelines. Two animals were excluded throughout the study; one mouse died during the CT scan and another had an incomplete perfusion. All described procedures were approved by the Uppsala County Animal Ethics board (5.8.18–20401/2020) following the legislation and regulations of the Swedish Animal Welfare Agency and European Communities Council Directive of 22 September 2010 (2010/63/EU).

Radiolabeling

The Chloramine-T method was used to radiolabel the antibodies by direct iodination with iodine-125 (^{125}I) (half-life 59.5 days) [45]. The antibody was mixed with [^{125}I]NaI (Perkin-Elmer Inc Waltham, MA, USA) and 5 μg (200 μM in PBS) Chloramine-T (Sigma Aldrich) in filtered PBS. After 90 s, the reaction was quenched by the addition of 10 μg (440 μM in PBS) sodium metabisulfite (Sigma Aldrich). On average, 95.5 ± 75 μg of antibody was labeled with 14.2 ± 9.5 MBq of ^{125}I . The resulting product was separated from free iodine and low molecular weight products using Zeba spin desalting columns (7 K MWCO, 0.5 mL, 89882, Thermo Fisher) or diluted to 500 μl with PBS and passed through a NAP-5 size exclusion column (5 kDa cutoff, GE Healthcare, Uppsala, Sweden) with a total elution volume of 1 mL PBS. The average radiochemical yield was $69.6 \pm 10.0\%$.

For the PET study, 75.4 MBq of [^{124}I]NaI (half-life 4.2 days) (Advanced Center Oncology Macerata, Montecosaro, Italy) was preincubated with 100 μM NaI (3.4 μM in final volume), for 15 min. The iodine solution was neutralized with 36 μl 0.5% acetic acid (83.3 mM) and 26 μl 10x PBS, before addition of 420 μg of IgG-scFv₂ (5.6 $\mu\text{g}/\text{MBq}$) in filtered PBS and 38 μg Chloramine-T (Sigma Aldrich) to a final reaction volume of 517 μl . After 120 s, the reaction was quenched by the addition of 76 μg sodium metabisulfite (Sigma Aldrich). The reaction mixture was purified with a NAP-5 size-exclusion column (5 kDa cutoff, GE Healthcare, Uppsala, Sweden) with a total elution volume of 1 mL PBS. This yielded in 58 MBq of: [^{124}I]IgG-scFv₂ with a radiochemical purity (RCP) >99%, radiochemical yield (RCY) of 77% and specific activity (As) of 0.14 MBq/ μg . RCP was assessed using radio-TLC on iTLC-SG paper (Agilent, SGI0001) with 70% acetone in water as the mobile phase. The retention factors (Rf) were: [^{124}I]IgG-scFv₂: Rf = 0, Free [^{124}I]Na: I Rf = 1.

In vitro stability of [^{125}I]IgG-scFv₂ was assessed in PBS at 4 °C and 37 °C, and in mouse plasma at 37 °C. Stability was analyzed by iTLC (mobile phase 70% acetone in water) immediately after purification and after 3 days of incubation, in line with the end-point of the ex vivo and PET studies. In vivo plasma stability of [^{125}I]IgG-scFv₂ was evaluated in App^{NL-G-F} and WT mice injected with the radiolabeled antibody. Plasma samples were collected 3 days p.i. and analyzed by iTLC using the same procedure as described above. RCP was calculated as the percentage of radioactivity retained at the origin, representing intact antibody, relative to total radioactivity on the strip. For in vitro and in vivo stability testing results, please see Supplementary Table S2.

To ensure that the binding affinity of the antibodies had not been affected by the radiolabeling, indirect ELISAs were performed (see Enzyme-linked immunosorbent assays (ELISA) in Materials and methods).

Ex vivo study of ^{125}I -iodinated bispecific antibodies

Mice, under light isoflurane anesthesia, were intravenously (i.v.) injected via the tail vein with 0.4 mg/kg, corresponding to 1.2 ± 0.3 MBq (Supplementary Table S1). Using a syringe needle, the tip of the tail vein was pricked and a blood sample (8 μL) was collected in a capillary tube at the following time points after injection: 30 min, 1, 2, 4, 6, 24 and 48 h. The mice were anesthetized with isoflurane 2, 24, 48–72 h after injection, and a terminal blood sample was taken from the heart, followed by transcardial perfusion with 0.9% NaCl. The terminal blood sample was placed in an Eppendorf tube prepared with heparin. The tube was centrifuged for 5 min at $10,000 \times g$ at 4 °C. Plasma was separated from the blood cells by aspiration. To investigate biodistribution of the radiolabeled antibodies, the brain, lung, liver, kidney, heart, pancreas, spleen, thyroid, skull, muscle, bone and urine, were harvested. The brain was divided into left and right hemispheres, and the left hemisphere was further divided into cerebrum and cerebellum. The brain samples were kept at -80 °C until further analysis. The radioactivity of all samples was measured with a γ -counter (2480 WizardTM, Wallac Oy PerkinElmer, Turku, Finland). Antibody concentrations were expressed as percent of injected dose per gram tissue (%ID/g). A separate group of six App^{NL-G-F} mice was used to study the binding specificity of IgG-scFv₂ to TREM2. Half of the mice were administered isotopically unmodified IgG-scFv₂ at a dose of 20 mg/kg, i.e. a 50-fold higher dose than the tracer dose used for the ex vivo uptake studies described above. Four days later, all six animals were administered an i.v. tracer dose of [^{125}I]IgG-scFv₂ corresponding to 1.8 ± 0.3 MBq (Supplementary Table S1). The brain was isolated at 72 h p.i. as described above. Sagittal brain sections, 20 μm , were prepared for ex vivo autoradiography and exposed to phosphor-imaging plates (Fujifilm) for two weeks. Plates were read with an Amersham Typhoon IP phosphor imager (GE Healthcare), at a resolution of 50 μm , and the images were converted to a false color scale (Royal) in ImageJ (1.54p, Fiji).

In vivo PET study with ^{124}I -iodinated bispecific antibodies

One day prior to the injection of [^{124}I]IgG-scFv₂, the mice to be scanned were given 0.5% NaI in their drinking water to reduce thyroidal uptake of ^{124}I . App^{NL-G-F} and WT mice ($n = 8$) were injected with 1 mg/kg corresponding to 6.3

± 1.0 MBq [^{124}I]IgG-scFv₂ (Supplementary Table S1). After the injection, NaI concentration in the drinking water was decreased to 0.2% NaI. Blood samples (8 μL) were obtained from the tail vein at the following time points after injection: 30 min, 1, 2, 4, 6, 24 and 48 h.

At 72 h after injection, the mice were anesthetized with 3% sevoflurane and scanned in triplicates for 120 min. The scans were performed in a preclinical nanoScan PET/MRI system (Mediso Medical Imaging Systems, Budapest, Hungary) followed by a CT in a preclinical nanoScan SPECT/CT (Mediso Medical Imaging Systems, Budapest, Hungary). After the scans, the mice were perfused, and the radioactivity in the brains and organs was measured by γ -counting according to the procedure described for the ex vivo studies. Images from the Mediso system were reconstructed using a Tera-TomoTM 3D algorithm (Mediso Medical Imaging Systems) with 4 iterations and 6 subsets. All subsequent image processing was performed with Amide version 1.0.6 [46]. PET and CT scans were manually aligned with a T2-weighted mouse brain atlas [47] to quantify activity in regions of interest. Brain regions used for analysis were whole brain, cortex, thalamus, caudate, hippocampus, and cerebellum.

Brain tissue extraction

The left cerebrum from the injected mice were homogenized with a Precellys Evolution (Bertin Technologies) (4×10 s at 5500 rpm) at a 1:5 weight/volume ratio in Tris-buffered saline with 1% Triton-X (TBST) with complete protease inhibitor (Sigma). After centrifugation, 2 h at $16,000 \times g$, the supernatant was immediately removed and frozen. Pellets from TBST homogenization were dissolved in 70% formic acid (FA) and centrifuged at $16,000 \times g$ for 1 h before collecting the supernatant.

To investigate TREM2 concentrations in brain tissue samples, a sandwich ELISA was performed using half-area 96-well plates (Corning inc.). Plates were coated with primary antibody AF1729 (0.5 $\mu\text{g}/\text{mL}$, R&D Systems) in PBS and incubated overnight at 4 °C. Plates were then blocked with 1% BSA for 3 h at RT, on a shaker. Brain TBST homogenate samples, diluted 1:50 in ELISA incubation buffer, were loaded in duplicates and incubated overnight at 4 °C. Secondary antibody BAF1729 (0.5 $\mu\text{g}/\text{mL}$, R&D Systems) and HRP-conjugated streptavidin (1:3000, Mabtech AB, Nacka, Sweden) were diluted in ELISA incubation buffer. K blue aqueous TMB substrate (Neogen Corp., Lexington, USA) was used to develop ELISA signals and the reaction was stopped with 1 M H₂SO₄. The plates were read with a spectrophotometer at 450 nm.

To measure A β 38, A β 40, and A β 42 concentrations in FA-extracted brain homogenate from App^{NL-G-F} mice, the

V-PLEX[®] A β peptide panel 1 (6E10) immunoassay (Meso Scale Discovery, K15200E) was used. Samples were neutralized with 2 M Tris and diluted 1:10 000 in assay diluent before being loaded in duplicate onto pre-coated and blocked 96-well plates together with the secondary A β antibody 6E10 conjugated to a SULFO-TAG for electro-chemiluminescent detection. After 2 h of incubation, plates were washed with PBS containing 0.05% Tween, and MSD read buffer was added. Plates were read with a MESO QuickPlex SQ instrument (Meso Scale Discovery).

Statistical analyses

Data are presented mean \pm standard deviation (SD). The Shapiro-Wilk test was used to assess the normality of the data distribution. For normally distributed data, Student's t-test, one-way ANOVA followed by Tukey's multiple comparisons test or two-way ANOVA followed by Šidák's multiple comparisons test were used to correct for multiple comparisons. For non-parametric datasets, Mann Whitney test, Kruskal-Wallis test followed by Dunn's multiple comparisons test was applied. Correlations were analyzed using Pearson correlation tests or Spearman correlation tests (r), and simple linear regression (R^2). All tests were two-tailed, with a significance level set at 95%. Statistically significant differences were defined as follows: p-value < 0.05 (*), p-value < 0.01 (**), p-value < 0.001 (***), p-value < 0.0001 (****). Graphs and statistical analyses were performed using GraphPad Prism version 10.4.0 (GraphPad Software, San Diego, California, USA) and in BioRender.com.

Results

The bispecific antibody formats showed different binding profiles to TfR and TREM2 in vitro

Six novel anti-TREM2 antibody formats were produced, with three of the constructs carrying the LALA-PG mutation to attenuate effector functions in vivo (Fig. 1) [43]. The formats lacking the LALA-PG mutation, IgG^{wt} and IgG^{wt}-scFv₂, were not carried forward as their brain uptake was lower than their mutated counterpart (Supplementary Fig. S1a, b). IgG-scFv₂ showed the strongest binding to murine TREM2 protein, followed by IgG-scFab and scFv-VHH (Fig. 2a). In line with reports of 14D3 preferentially binding human TREM2 protein, all three constructs had comparable in vitro binding to human TREM2 (Fig. 2b) [39]. The three TfR-binders differed somewhat in their affinity to murine TfR protein in direct ELISA (Fig. 2c). IgG-scFv₂, with bivalent scFv of the TfR antibody 8D3 [27, 41], had the strongest TfR protein affinity, followed by the scFv-VHH, linked

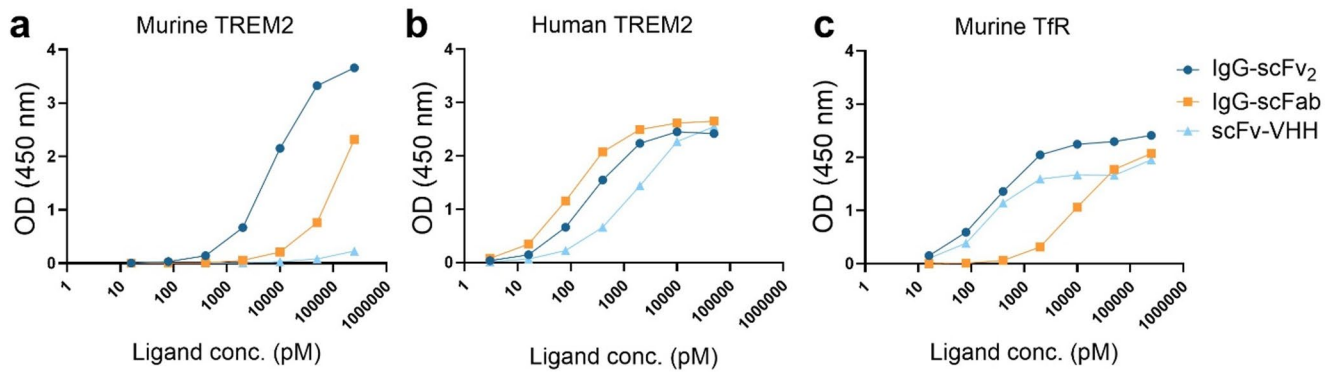


Fig. 2 Binding of IgG-scFv₂, IgG-scFab, and scFv-VHH to (a) murine TREM2 protein, (b) human TREM2 protein and (c) murine transferrin receptor (TfR) protein, measured by absorbance in ELISA

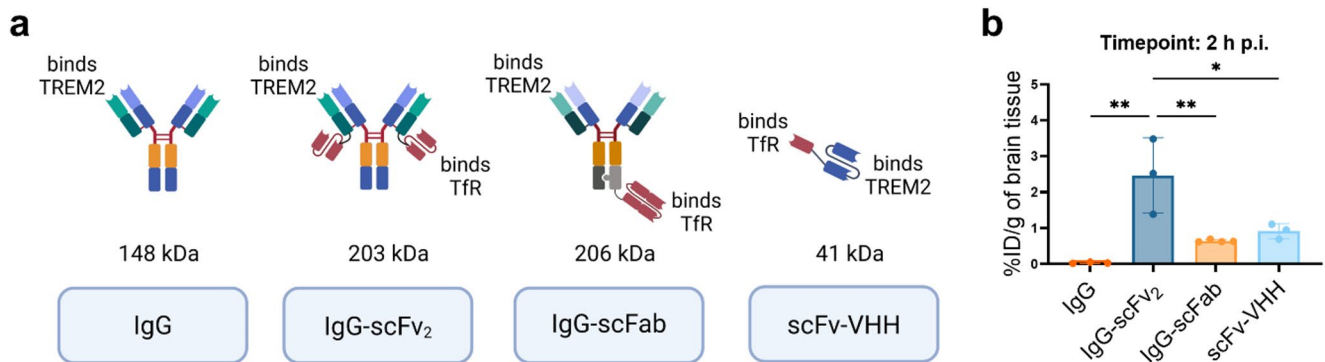


Fig. 3 (a) Schematic illustration of the anti-TREM2 antibody formats that were carried forward. (b) Brain concentration of ¹²⁵I-labeled bispecific anti-TREM2 antibodies, expressed as percentage of injected

dose per gram of brain tissue 2 h post injection. WT $n = 13$. One-way ANOVA followed by Tukey's multiple comparisons test ($*p < 0.05$, $**p < 0.01$), mean \pm SD

to a TfR nanobody [42]. IgG-scFab, carrying a monovalent scFab of 8D3 showed the weakest TfR binding [28].

Bispecific antibody [¹²⁵I]IgG-scFv₂ demonstrated highest ex vivo brain retention in transgenic mice

All bispecific anti-TREM2-anti-TfR constructs were able to cross the BBB and enter the brain in WT mice two hours post injection (p.i.) (Fig. 3). In comparison to the control IgG without a TfR-binder, IgG-scFv₂ displayed 67-fold higher brain concentrations, followed by a 25-fold and 17-fold increased brain concentration for scFv-VHH and IgG-scFab, respectively (Fig. 3b).

Once the ability of the bispecific constructs to cross the BBB had been evaluated in WT mice, App^{NL-G-F} mice were added and the experimental time points were extended to 48 and 72 h p.i. The blood clearance of the bispecific constructs was found to be format-dependent rather than genotype-dependent, with the smallest scFv-VHH exhibiting faster blood clearance p.i. (Fig. 4a). At both 48 h and 72

h p.i., IgG-scFv₂ was able to distinguish App^{NL-G-F} mice from age-matched WT mice (Fig. 4b, d). App^{NL-G-F} mice also had a significantly higher brain-to-blood concentration ratio than the WT mice at 72 h p.i. (Fig. 4e). The brain concentration of IgG-scFab did not significantly differ between genotypic groups at any of the timepoints (Fig. 4b, d). The scFv-VHH displayed higher brain concentrations and a higher brain-to-blood ratio in App^{NL-G-F} mice than in WT mice at 48 h, but not at 24 h (Supplementary Fig. S1c) and 72 h p.i. (Fig. 4b-e). Peripheral biodistribution at 2, 48 and 72 h p.i. is shown in Supplementary Fig. S2.

To investigate the binding specificity of IgG-scFv₂ to TREM2, App^{NL-G-F} mice were administered a pre-saturating dose of IgG-scFv₂. The pre-treated mice exhibited significantly lower brain concentrations of [¹²⁵I]IgG-scFv₂ at 72 h p.i. compared to the untreated group of App^{NL-G-F} mice, indicating a blocking effect (Fig. 4f). This effect was further confirmed by ex vivo autoradiography, which showed a markedly reduced [¹²⁵I]IgG-scFv₂ signal in sagittal brain sections from pre-treated mice (Fig. 4g).

In vivo PET-imaging with IgG-scFv₂ detected elevated TREM2 levels in App^{NL-G-F} 72 h post injection

As [¹²⁵I]IgG-scFv₂ achieved the highest brain concentration and demonstrated the most significant distinction between AD and WT mice in ex vivo studies, this format was selected for in vivo PET imaging of the TREM2 protein. Radiolabeling IgG-scFv₂ with the PET-compatible radionuclide ¹²⁴I had a relatively minor effect on its binding affinity to either murine TREM2 protein or murine TfR protein (Fig. 5a, b).

App^{NL-G-F} mice and WT mice were scanned 72 h p.i. of [¹²⁴I]IgG-scFv₂ (Fig. 5c). In line with the previous ex vivo results, PET-imaging showed that App^{NL-G-F} mice had significantly higher [¹²⁴I]IgG-scFv₂ brain concentrations than the WT mice measured in the whole brain, cortex, thalamus, caudate and hippocampus (Fig. 5d–f). This was further corroborated by the post mortem ex vivo measured brain concentration (Fig. 5g). App^{NL-G-F} mice and WT mice did not differ in blood clearance or peripheral organ retention of [¹²⁴I]IgG-scFv₂ (Fig. 5h, i).

Elevated PET signals correspond to elevated TREM2 levels in App^{NL-G-F} mice

To confirm that the retention of the bispecific anti-TREM2-anti-TfR constructs and the in vivo visualization of TREM2 using PET-imaging was correlated to increased TREM2 levels, the concentration of TREM2 was measured in the TBST-soluble fraction of brain homogenate prepared from all included animals. App^{NL-G-F} mice displayed considerably higher brain concentrations of TREM2 than WT mice (Fig. 6a). Significant correlations between TREM2 concentrations in brain homogenate and bispecific antibody brain concentrations were found for ¹²⁵I- and ¹²⁴I-labeled IgG-scFv₂ at 72 h p.i. (Fig. 6b, c).

TREM2 correlates with Aβ load in App^{NL-G-F} mice

In addition to TREM2, Aβ load was measured in the FA-soluble brain homogenate fractions prepared from App^{NL-G-F} mice. Out of the three measured Aβ species, Aβ₃₈ was the predominant isoform, with a 28-fold higher concentration than Aβ₄₀ and 2.7-fold higher concentration than Aβ₄₂ (Fig. 7a). The correlations between TREM2 and Aβ were found to be significant for Aβ₃₈ and Aβ₄₀, but not Aβ₄₂ (Fig. 7b–d). However, these correlations were mainly driven by one mouse with highly elevated Aβ concentrations. When this mouse was excluded from data analysis, only the correlation between TREM2 and Aβ₃₈ remained statistically significant.

Discussion

Several point mutations in the extracellular domain of TREM2—where the 14D3 antibody used in this study binds—have been linked to neurodegenerative disorders, underscoring the critical role of TREM2 in maintaining brain health and homeostasis [48, 49]. Further, sTREM2 levels in cerebrospinal fluid have been reported to be increased in AD [50]. Therefore, the reported implications of TREM2 in AD pathology have placed the protein at the forefront of efforts to both monitor and treat neuroinflammation using biologics. However, at present, there are no radioligands available for in vivo diagnostic evaluation of brain TREM2 levels, and only suboptimal radioligands available for detection of activated microglia or neuroinflammation in general.

In this study, we produced and compared radiolabeled bispecific anti-TREM2 antibody constructs based on the 14D3 antibody fused with three different TfR binders. Among these, the bivalent IgG-scFv₂ format exhibited the highest brain retention in transgenic mice with AD pathology, establishing it as the most effective diagnostic radioligand among the formats tested. Notably, at 72 h p.i., the radioligand [¹²⁵I]IgG-scFv₂ differentiated aged App^{NL-G-F} mice from age-matched WT controls based on ex vivo radioactivity measurements of isolated brain samples. Moreover, when labeled with the PET-compatible radionuclide iodine-124, [¹²⁴I]IgG-scFv₂ distinguished App^{NL-G-F} mice from WT mice also through PET imaging.

Additionally, higher brain TREM2 levels were detected in App^{NL-G-F} mice compared to WT mice, and a significant correlation was found between elevated TREM2 and the increased PET signal. The App^{NL-G-F} mouse model is characterized by robust and abundant Aβ pathology at a relatively early age [44]. By 14 months, the App^{NL-G-F} mice have substantial brain concentrations of Aβ₃₈, and a high Aβ₄₂ to Aβ₄₀ ratio distinctive of the Beyreuther/Iberian mutation. This pathology is accompanied by neuroinflammation, including microglial activation. TREM2's expression on the microglial cell surface enables it to act as a sensor—directly interacting with Aβ isoforms. TREM2 has a high affinity for Aβ oligomers, especially soluble Aβ₄₂, and facilitates Aβ internalization [51]. Studies in TREM2-deficient mice have also emphasized the importance of TREM2 in compacting Aβ into a less harmful form [23]. The TREM2-mediated effects in AD pathophysiology, together with its extracellular location, make it a well-suited focal point for microglia-specific PET-imaging.

PET radioligands are ideally based on molecules with fast pharmacokinetics. For example, fast elimination of the radioligand from blood contributes to higher imaging contrast for brain targets. In this study, a smaller scFv-VHH

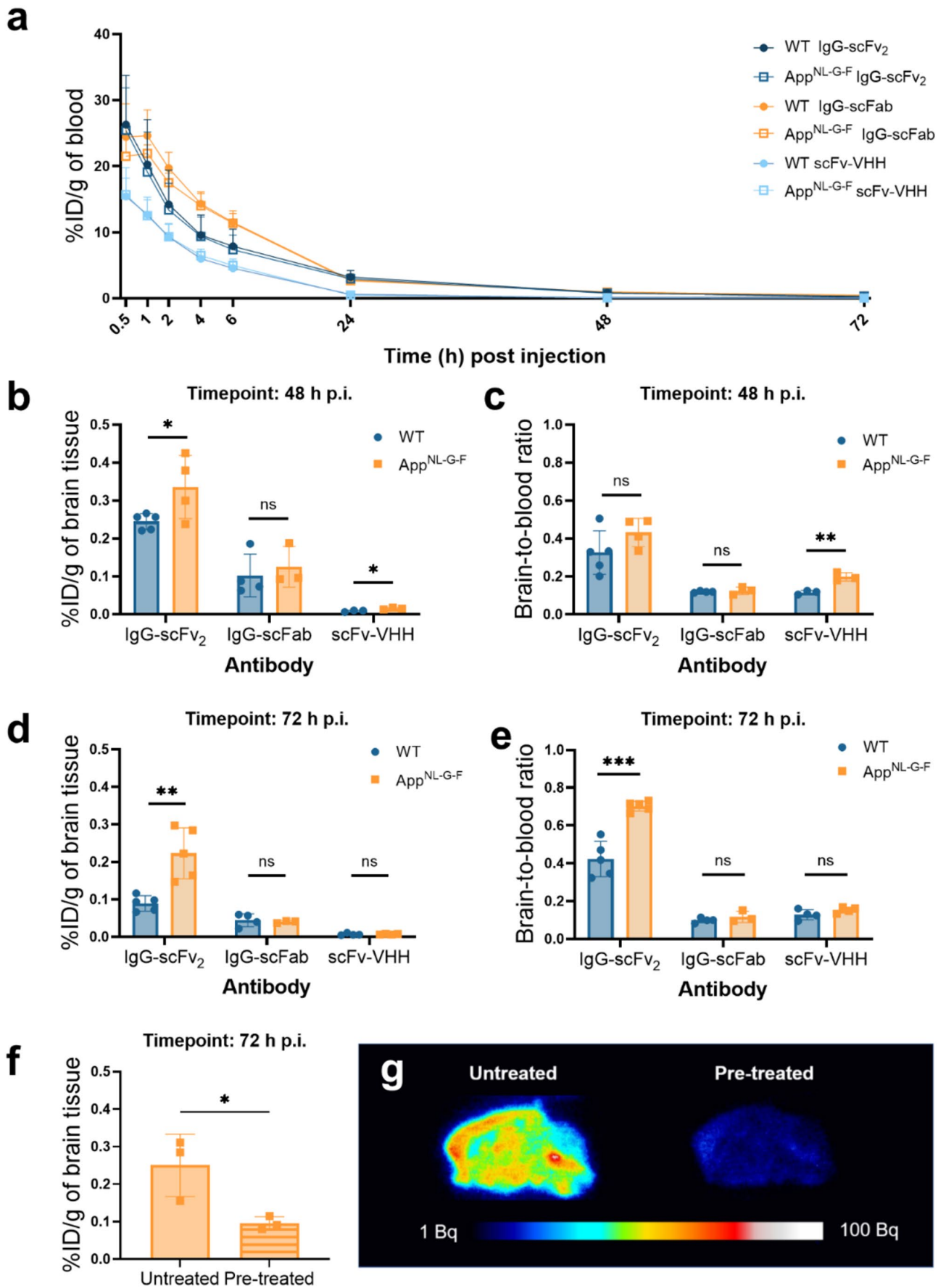


Fig. 4 (a) Blood-time concentration (%ID/g of blood) curves up to 72 h post injections (p.i.). Brain concentration of ^{125}I -labeled bispecific anti-TREM2 antibodies 48 h p.i. (b) expressed as percentage of injected dose per gram of brain tissue (%ID/g of brain) and as (c) brain-to-blood concentration ratio (App^{NL-G-F} $n=10$, WT $n=12$). Brain concentration of ^{125}I -labeled bispecific anti-TREM2 antibodies 72 h p.i. (d) expressed as %ID/g of brain and as (e) brain-to-blood concentration ratio (App^{NL-G-F} $n=12$, WT $n=13$). (f) Brain concentration of [^{125}I]IgG-scFv₂ 72 h p.i. in App^{NL-G-F} mice untreated ($n=3$) or pre-treated ($n=3$) with a 50-fold higher dose of IgG-scFv₂ four days prior. (g) Representative ex vivo autoradiography showing binding of [^{125}I]IgG-scFv₂ 72 h p.i. in sagittal brain sections prepared from untreated and pre-treated litter mates. Student's t-test (* $p < 0.05$, ** $p < 0.01$, *** $p < 0.001$), mean \pm SD

format was therefore evaluated, which indeed displayed faster elimination from blood. Accordingly, the brain concentration and brain-to-blood concentration ratio of [^{125}I]scFv-VHH differed between App^{NL-G-F} and WT mice as early as 48 h, i.e. one day earlier than with the larger [^{125}I]IgG-scFv₂ construct. However, total brain concentrations were substantially lower with the smaller [^{125}I]scFv-VHH compared to the larger [^{125}I]IgG-scFv₂. Several factors may explain this: first, the different TfR binder may have contributed to less efficient transport across the BBB. Nevertheless, the concentration of 1% ID/g of brain tissue at 2 h p.i. is relatively good and has proven sufficient for other antibody-based radioligands targeting A β [52]. Second, the monovalent form of 14D3 has lower affinity for TREM2, which could decrease retention, especially in mice, as this study and others have shown that 14D3 binds more effectively to human TREM2 than murine TREM2. While the lower affinity of 14D3 for murine TREM2 compared to human TREM2 (76% protein homology) is a limitation of this study, it represents an advantage for future clinical studies, increasing the likelihood of successful translation to clinical applications. Thus, from a translational perspective, the small scFv-VHH should not be ruled out as a potential future diagnostic for humans, but its retention was not enough for detection of elevated TREM2 in mice. The third evaluated construct, IgG-scFab, was based on the Roche Brain Shuttle format [28], comprising a monovalent TfR binder and a full-sized 14D3 IgG. Its initial BBB transport, and consequently, the 2 h concentration, was lower than that of the bivalent TfR binder IgG-scFv₂, yet similar to that of the monovalent scFv-VHH. Interestingly, IgG-scFab showed lower affinity for murine TREM2 than IgG-scFv₂, despite both constructs using the same format for the 14D3 moiety. No such difference was observed in binding to human TREM2. Therefore, although this construct did not distinguish high from low TREM2 levels in mice, it may be effective in detecting elevated TREM2 in humans.

Preclinical PET imaging of TREM2 has previously been explored with a radiolabeled bispecific TREM2-TfR antibody, created by chemically conjugating antibody AF1729, which primarily binds to sTREM2, the soluble form of TREM2, and scFv8D3 [38]. In Meier et al. (2021), tg-ArcSwe mice showed increased retention compared to WT controls based on ex vivo radioactivity measurements in perfused brains; however, this difference was insufficient to distinguish the genotypes by PET imaging. More recently, TREM2 levels were detected using a bispecific antibody in the 5xFAD mouse model expressing human TfR [x viv39]. The study utilized a copper-64-labeled 4D9 antibody incorporating a region in the Fc domain that binds to human TfR, following Denali's Antibody Transport Vehicle (ATV) format. PET imaging with ^{64}Cu -labeled ATV:4D9, targeting both soluble and membrane-bound TREM2, gave a pronounced cortical radioligand uptake at 20 h p.i. The study reported higher brain concentrations in 5xFAD mice than in WT at this time point. However, the study also reported high blood concentrations of the radioligand. Furthermore, higher blood concentrations were observed in 5xFAD mice compared to WT mice. At elevated blood concentrations, the radioactivity in the blood volume of the brain can constitute a significant portion of the total PET signal. This could represent a major contributing factor, independent of TREM2 levels, to the increased radioactivity detected in the 5xFAD brain compared to WT when using ^{64}Cu -labeled ATV:4D9 PET. Notably, the brain-to-blood ratio of ^{64}Cu -labeled ATV:4D9 was observed to be very similar between 5xFAD and WT mice. In contrast, this ratio was significantly elevated in App^{NL-G-F} mice compared to WT when using the radiolabeled 14D3-based IgG-scFv₂ in the present study. Unlike 4D9, the 14D3 antibody specifically targets membrane-bound TREM2. This is likely to enhance the retention of the radioligand in the brain by preventing its clearance through the natural elimination of sTREM2. For a more direct comparison between these two radioligands it would be interesting to use a ^{64}Cu -labeled version of the IgG-scFv₂. The above-mentioned study with sTREM2-targeted antibody AF1729 also suggests that binding to sTREM2 is suboptimal, as the retention of the radioligand is likely influenced by the turnover of sTREM2 [38]. Furthermore, Shojaei et al. (2024) included in vitro autoradiography on human brain sections using the 14D3 antibody in the bispecific ATV format, further supporting the clinical translatability of the 14D3-based [^{124}I]IgG-scFv₂ findings presented in this present study.

To conclude, we have produced and evaluated three bispecific anti-TREM2 antibody formats that were able to cross the BBB by TfR mediated transcytosis and thus

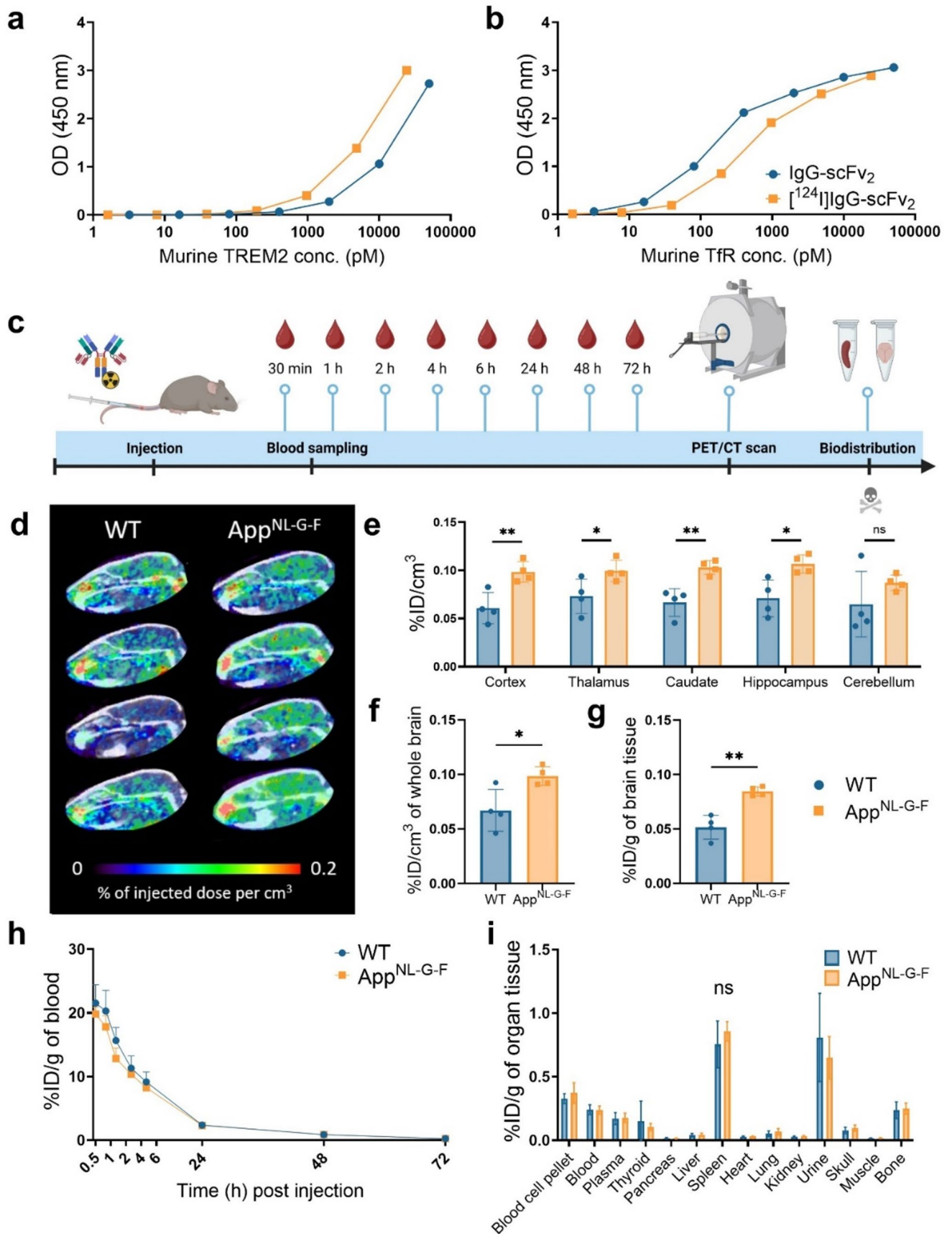


Fig. 5 Radiolabeling of IgG-scFv₂ with ¹²⁴I did not significantly alter the (a) binding to murine TREM2 protein or (b) murine TfR. (c) Experimental workflow for PET-imaging of [¹²⁴I]IgG-scFv₂ 72 h post injection (p.i.). Blood samples were collected from the tail vein at 30 min, 1 h, 2 h, 4 h, 6 h, 24 h, 48 h p.i. Terminal blood samples were collected from the heart prior to transcardial perfusion 72 h p.i. Radioactivity in the collected organs was measured using a γ -counter. (d-f) PET-imaging showed significantly higher in vivo brain concentration of [¹²⁴I]IgG-scFv₂ in App^{NL-G-F} mice in comparison to WT mice, (g) which was confirmed by ex vivo measurements. (h) Blood-time concentration (%ID/g of blood) and (i) organ biodistribution 72 h p.i. (App^{NL-G-F} *n* = 4, WT *n* = 4). Student's t-test, Two-way ANOVA followed by Šidák's multiple comparisons test (**p* < 0.05, ***p* < 0.01), mean \pm SD

achieve high brain concentrations. The constructs showed binding to both murine and human TREM2 in vitro. Using the bispecific radioimmunoconjugate [¹²⁴I]IgG-scFv₂, PET imaging of TREM2 in the living brain was successful. Utilizing PET imaging to visualize TREM2-associated microglial activation will hold significant diagnostic promise for AD patients and offers a non-invasive method to assess the efficacy of new anti-inflammatory drug candidates.

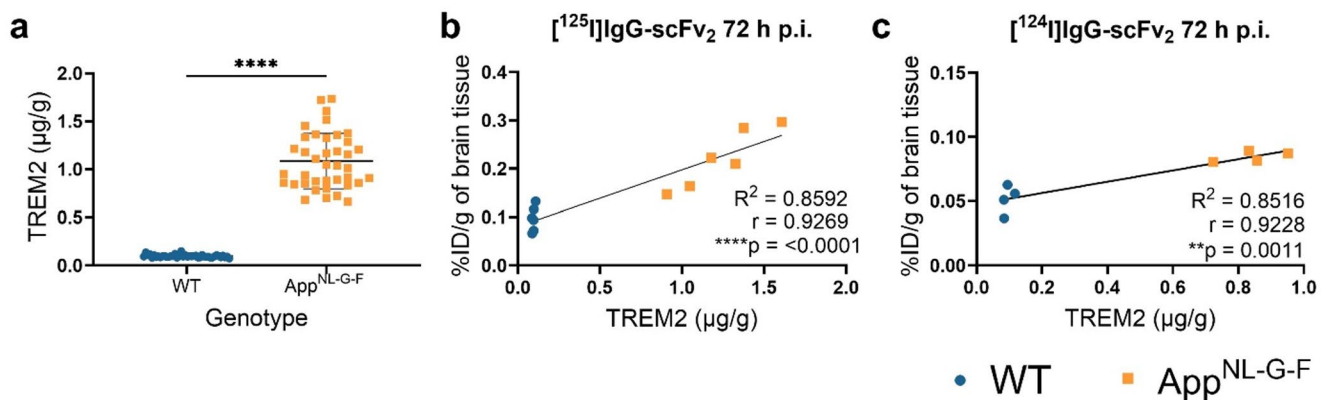


Fig. 6 (a) TREM2 levels in TBST-extracted brain homogenate were significantly higher in the App^{NL-G-F} mice in comparison to WT mice (App^{NL-G-F} *n* = 39, WT *n* = 42). Significant correlations between TREM2 concentrations in brain homogenate and brain concentration (%ID/g) of injected antibody were detected at 72 h p.i. of (b)

(c) [¹²⁵I]IgG-scFv₂ (App^{NL-G-F} *n* = 6, WT *n* = 6) and (c) [¹²⁴I]IgG-scFv₂ (App^{NL-G-F} *n* = 4, WT *n* = 4). Mann Whitney test, Pearson correlation test (*r*), Simple linear regression (R²) (***p* < 0.01, *****p* < 0.0001), mean \pm SD

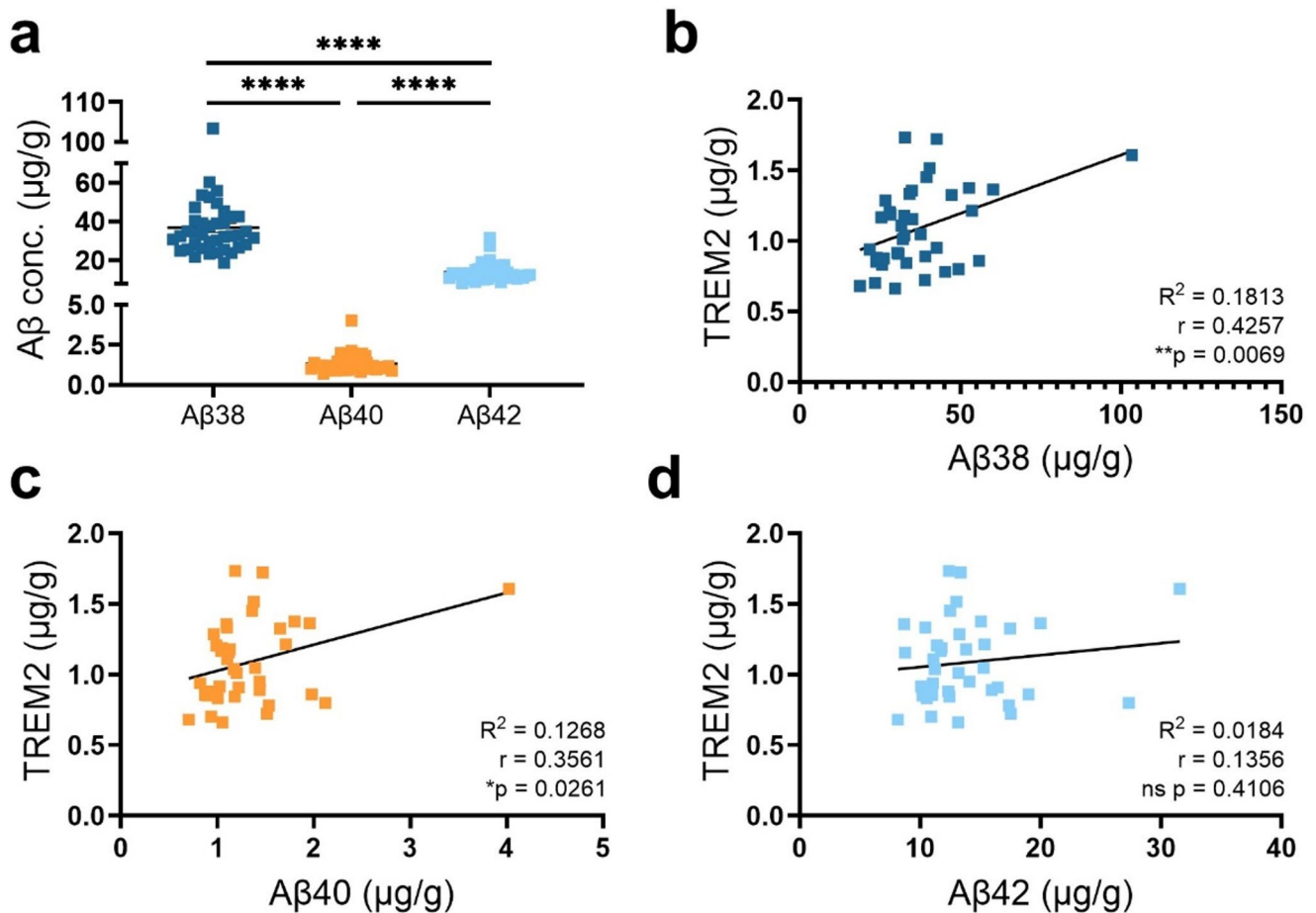


Fig. 7 (a) Aβ38, Aβ40, and Aβ42 concentrations were measured in formic acid-extracted brain homogenate from *App^{NL-G-F}* mice ($n = 39$). Significant correlations between TREM2 concentration and concentration of (b) Aβ38 and (c) Aβ40 were detected in the brain homogenate.

(d) Levels of TREM2 and Aβ42 did not correlate. Kruskal-Wallis test followed by Dunn's multiple comparisons test. Pearson correlation test (r), Simple linear regression (R^2) ($*p < 0.05$, $**p < 0.01$, $****p < 0.0001$), mean \pm SD

Supplementary Information The online version contains supplementary material available at <https://doi.org/10.1007/s00259-025-07358-0>.

Acknowledgements The molecular imaging work in this study was performed at the Preclinical PET-MRI Platform, a research infrastructure at Uppsala University, Sweden. We would like to thank Takashi Saito and Takaomi Saido at RIKEN Center for Brain Science, for the development of the *App^{NL-G-F}* model used in the present study.

Authors' contributions AD, SR, DS and SS contributed to the conception and design of the study; AD, SR, XA, NB, SLB, DS and SS contributed to the acquisition of data. AD, SLB, DS and SS contributed to the analysis of data; AD, DS and SS contributed to drafting the text or preparing the figures. All authors read and approved the final manuscript.

Funding Open access funding provided by Uppsala University. This work was supported by grants from the Swedish Research Council (2021–01083 and 2021–03524), Parkinsonfonden, Alzheimerfon-

den, Hjärfonden, Åhlenstiftelsen, Stiftelsen för gamla tjänarinnor, Stohnes stiftelse, and Konung Gustaf V: s och Drottning Victorias frimurarestiftelse. The funding organizations did not take part in designing the study, in collecting, analysing, or interpreting the data, or in writing the manuscript.

Data availability The datasets used and/or analysed during the current study are available from the corresponding author on reasonable request.

Declarations

Ethics approval All described procedures were approved by the Uppsala Country Animal Ethics board (5.8.18-20401/2020), following the rules and regulations of the Swedish Animal Welfare Agency and complied with the European Communities Council Directive of 22 September 2010 (2010/63/EU). The current study did not include patient information.

Consent for publication Not applicable.

Clinical trial number Not applicable.

Competing interests The authors declare that they have no conflict of interest.

Open Access This article is licensed under a Creative Commons Attribution 4.0 International License, which permits use, sharing, adaptation, distribution and reproduction in any medium or format, as long as you give appropriate credit to the original author(s) and the source, provide a link to the Creative Commons licence, and indicate if changes were made. The images or other third party material in this article are included in the article's Creative Commons licence, unless indicated otherwise in a credit line to the material. If material is not included in the article's Creative Commons licence and your intended use is not permitted by statutory regulation or exceeds the permitted use, you will need to obtain permission directly from the copyright holder. To view a copy of this licence, visit <http://creativecommons.org/licenses/by/4.0/>.

References

- Shcherbinin S, Evans CD, Lu M, Andersen SW, Pontecorvo MJ, Willis BA, et al. Association of amyloid reduction after Donanemab treatment with Tau pathology and clinical outcomes: the TRAILBLAZER-ALZ randomized clinical trial. *JAMA Neurol*. 2022. <https://doi.org/10.1001/jamaneurol.2022.2793>.
- van Dyck CH, Swanson CJ, Aisen P, Bateman RJ, Chen C, Gee M, et al. Lecanemab in early Alzheimer's disease. *N Engl J Med*. 2023. <https://doi.org/10.1056/NEJMoa2212948>.
- Leng F, Edison P. Neuroinflammation and microglial activation in Alzheimer disease: where do we go from here? *Nat Rev Neurol*. 2021. <https://doi.org/10.1038/s41582-020-00435-y>.
- Heneka MT, Carson MJ, El Khoury J, Landreth GE, Brosseron F, Feinstein DL, et al. Neuroinflammation in Alzheimer's disease. *Lancet Neurol*. 2015. [https://doi.org/10.1016/S1474-4422\(15\)70016-5](https://doi.org/10.1016/S1474-4422(15)70016-5).
- Fan Z, Brooks DJ, Okello A, Edison P. An early and late peak in microglial activation in Alzheimer's disease trajectory. *Brain*. 2017. <https://doi.org/10.1093/brain/aww349>.
- Hamelin L, Lagarde J, Dorothée G, Potier MC, Corlier F, Kuhnast B, et al. Distinct dynamic profiles of microglial activation are associated with progression of Alzheimer's disease. *Brain*. 2018. <https://doi.org/10.1093/brain/awy079>.
- Owen DR, Yeo AJ, Gunn RN, Song K, Wadsworth G, Lewis A, et al. An 18-kDa translocator protein (TSPO) polymorphism explains differences in binding affinity of the PET radioligand PBR28. *J Cereb Blood Flow Metab*. 2012. <https://doi.org/10.1038/jcbfm.2011.147>.
- Zanotti-Fregonara P, Pascual B, Rizzo G, Yu M, Pal N, Beers D, et al. Head-to-Head comparison of ¹¹C-PBR28 and ¹⁸F-GE180 for quantification of the translocator protein in the human brain. *J Nucl Med*. 2018. <https://doi.org/10.2967/jnumed.117.203109>.
- Vivash L, O'Brien TJ. Imaging microglial activation with TSPO PET: lighting up neurologic diseases?? *J Nucl Med*. 2016. <https://doi.org/10.2967/jnumed.114.141713>.
- Lee SH, Denora N, Laquintana V, Mangiatordi GF, Lopodota A, Lopalco A, et al. Radiosynthesis and characterization of [¹⁸F]BS224: a next-generation TSPO PET ligand insensitive to the rs6971 polymorphism. *Eur J Nucl Med Mol Imaging*. 2021. <https://doi.org/10.1007/s00259-021-05617-4>.
- Gouilly D, Saint-Aubert L, Ribeiro MJ, Salabert AS, Tauber C, Péran P, et al. Neuroinflammation PET imaging of the translocator protein (TSPO) in Alzheimer's disease: an update. *Eur J Neurosci*. 2022. <https://doi.org/10.1111/ejn.15613>.
- Liu Y, Jiang H, Qin X, Tian M, Zhang H. PET imaging of reactive astrocytes in neurological disorders. *Eur J Nucl Med Mol Imaging*. 2022. <https://doi.org/10.1007/s00259-021-05640-5>.
- Fowler JS, Logan J, Shumay E, Alia-Klein N, Wang GJ, Volkow ND. Monoamine oxidase: Radiotracer chemistry and human studies. *J Label Compd Radiopharm*. 2015. <https://doi.org/10.1002/jlcr.3247>.
- Rodriguez-Vieitez E, Saint-Aubert L, Carter SF, Almkvist O, Farid K, Schöll M, et al. Diverging longitudinal changes in astrocytosis and amyloid PET in autosomal dominant Alzheimer's disease. *Brain*. 2016. <https://doi.org/10.1093/brain/awv404>.
- Olsen M, Aguilar X, Sehlin D, Fang XT, Antoni G, Erlandsson A, et al. Astroglial responses to Amyloid-Beta progression in a mouse model of Alzheimer's disease. *Mol Imaging Biol*. 2018. <https://doi.org/10.1007/s11307-017-1153-z>.
- Kumar A, Fontana IC, Nordberg A. Reactive astrogliosis: A friend or foe in the pathogenesis of Alzheimer's disease. *J Neurochem*. 2023. <https://doi.org/10.1111/jnc.15565>.
- Kumar A, Koistinen NA, Malarte ML, Nennesmo I, Ingelsson M, Ghetti B, et al. Astroglial tracer BU99008 detects multiple binding sites in Alzheimer's disease brain. *Mol Psychiatry*. 2021. <https://doi.org/10.1038/s41380-021-01101-5>.
- Cui X, Qiao J, Liu S, Wu M, Gu W. Mechanism of TREM2/DAP12 complex affecting β -amyloid plaque deposition in Alzheimer's disease modeled mice through mediating inflammatory response. *Brain Res Bull*. 2021. <https://doi.org/10.1016/j.brainresbull.2020.10.006>.
- Li Y, Xu H, Wang H, Yang K, Luan J, Wang S. TREM2: potential therapeutic targeting of microglia for Alzheimer's disease. *Biomed Pharmacother*. 2023. <https://doi.org/10.1016/j.biopha.2023.115218>.
- Jonsson T, Stefansson H, Steinberg S, Jonsdottir I, Jonsson PV, Snaedal J, et al. Variant of TREM2 associated with the risk of Alzheimer's disease. *N Engl J Med*. 2013. <https://doi.org/10.1056/NEJMoa1211103>.
- Guerreiro R, Wojtas A, Bras J, Carrasquillo M, Rogava E, Majounie E, et al. Alzheimer genetic analysis group. TREM2 variants in Alzheimer's disease. *N Engl J Med*. 2013. <https://doi.org/10.1056/NEJMoa1211851>.
- Prokop S, Miller KR, Labra SR, Pitkin RM, Hoxha K, Narasimhan S, et al. Impact of TREM2 risk variants on brain region-specific immune activation and plaque microenvironment in Alzheimer's disease patient brain samples. *Acta Neuropathol*. 2019. <https://doi.org/10.1007/s00401-019-02048-2>.
- Meilandt WJ, Ngu H, Gogineni A, Lalehzadeh G, Lee SH, Srinivasan K, et al. Trem2 deletion reduces Late-Stage amyloid plaque accumulation, elevates the A β 42:A β 40 ratio, and exacerbates axonal dystrophy and dendritic spine loss in the PS2APP Alzheimer's mouse model. *J Neurosci*. 2020. <https://doi.org/10.1523/JNEUROSCI.1871-19.2019>.
- Schlepckow K, Kleinberger G, Fukumori A, Feederle R, Lichtenhaler SF, Steiner H, et al. An Alzheimer-associated TREM2 variant occurs at the ADAM cleavage site and affects shedding and phagocytic function. *EMBO Mol Med*. 2017. <https://doi.org/10.15252/emmm.201707672>.
- Filipello F, Goldsby C, You SF, Locca A, Karch CM, Piccio L. Soluble TREM2: innocent bystander or active player in neurological diseases? *Neurobiol Dis*. 2022. <https://doi.org/10.1016/j.nbd.2022.105630>.
- Yu YJ, Zhang Y, Kenrick M, Hoyte K, Luk W, Lu Y, et al. Boosting brain uptake of a therapeutic antibody by reducing its affinity for a transcytosis target. *Sci Transl Med*. 2011. <https://doi.org/10.1126/scitranslmed.3002230>.

27. Hultqvist G, Syvänen S, Fang XT, Lannfelt L, Sehlin D. Bivalent brain shuttle increases antibody uptake by monovalent binding to the transferrin receptor. *Theranostics*. 2017. <https://doi.org/10.7150/thno.17155>.
28. Niewoehner J, Bohrmann B, Collin L, Urich E, Sade H, Maier P, et al. Increased brain penetration and potency of a therapeutic antibody using a monovalent molecular shuttle. *Neuron*. 2014. <https://doi.org/10.1016/j.neuron.2013.10.061>.
29. Faresjö R, Bonvicini G, Fang XT, Aguilar X, Sehlin D, Syvänen S. Brain pharmacokinetics of two BBB penetrating bispecific antibodies of different size. *Fluids Barriers CNS*. 2021. <https://doi.org/10.1186/s12987-021-00257-0>.
30. Schlein E, Andersson KG, Dallas T, Syvänen S, Sehlin D. Reducing neonatal Fc receptor binding enhances clearance and brain-to-blood ratio of TfR-delivered bispecific amyloid- β antibody. *MAbs*. 2024. <https://doi.org/10.1080/19420862.2024.2339337>.
31. Sehlin D, Roshanbin S, Zachrisson O, Ingelsson M, Syvänen S. A brain-penetrant bispecific antibody lowers oligomeric alpha-synuclein and activates microglia in a mouse model of alpha-synuclein pathology. *Neurotherapeutics*. 2024. <https://doi.org/10.1016/j.neurot.2024.e00510>.
32. Bonvicini G, Syvänen S, Andersson KG, Haaparanta-Solin M, López-Picón F, Sehlin D. ImmunoPET imaging of amyloid-beta in a rat model of Alzheimer's disease with a bispecific, brain-penetrating fusion protein. *Transl Neurodegener*. 2022. <https://doi.org/10.1186/s40035-022-00324-y>.
33. de la Pagnon M, Syvänen S, Giedraitis V, Hooley M, Konstantinidis E, Meier SR, et al. Altered amyloid- β structure markedly reduces gliosis in the brain of mice harboring the Uppsala APP deletion. *Acta Neuropathol Commun*. 2024. <https://doi.org/10.1186/s40478-024-01734-x>.
34. Roshanbin S, Xiong M, Hultqvist G, Söderberg L, Zachrisson O, Meier S, et al. In vivo imaging of alpha-synuclein with antibody-based PET. *Neuropharmacology*. 2022. <https://doi.org/10.1016/j.neuropharm.2022.108985>.
35. Meier SR, Sehlin D, Roshanbin S, Falk VL, Saito T, Saido TC, et al. ^{11}C -PiB and ^{124}I -Antibody PET provide differing estimates of brain Amyloid- β after therapeutic intervention. *J Nucl Med*. 2022. <https://doi.org/10.2967/jnumed.121.262083>.
36. Sehlin D, Fang XT, Cato L, Antoni G, Lannfelt L, Syvänen S. Antibody-based PET imaging of amyloid beta in mouse models of Alzheimer's disease. *Nat Commun*. 2016. <https://doi.org/10.1038/ncomms10759>.
37. Sehlin D, Syvänen S. MINC faculty. Engineered antibodies: new possibilities for brain PET? *Eur J Nucl Med Mol Imaging*. 2019. <https://doi.org/10.1007/s00259-019-04426-0>.
38. Meier SR, Sehlin D, Hultqvist G, Syvänen S. Pinpointing brain TREM2 levels in two mouse models of Alzheimer's disease. *Mol Imaging Biol*. 2021. <https://doi.org/10.1007/s11307-021-01591-3>.
39. Shojaei M, Schaefer R, Schlepckow K, Kunze LH, Struebing FL, Brunner B, et al. PET imaging of microglia in Alzheimer's disease using copper-64 labeled TREM2 antibodies. *Theranostics*. 2024. <https://doi.org/10.7150/thno.97149>.
40. Haass C, Kleinberger G, Schlepckow K. TREM2 cleavage modulators and uses thereof. United States Patent US 10,941,200 B2. 9 Mar 2021.
41. Kissel K, Hamm S, Schulz M, Vecchi A, Garlanda C, Engelhardt B. Immunohistochemical localization of the murine transferrin receptor (TfR) on blood-tissue barriers using a novel anti-TfR monoclonal antibody. *Histochem Cell Biol*. 1998. <https://doi.org/10.1007/s004180050266>.
42. Cohen R, David M, Khrestchatsky M. Transferrin receptor-binding molecules, conjugates thereof and their uses. Patent WO 2020/144233 A1. 16 Jul 2020.
43. Lo M, Kim HS, Tong RK, Bainbridge TW, Vernes JM, Zhang Y, et al. Effector-attenuating substitutions that maintain antibody stability and reduce toxicity in mice. *J Biol Chem*. 2017. <https://doi.org/10.1074/jbc.M116.767749>.
44. Saito T, Matsuba Y, Mihira N, Takano J, Nilsson P, Itoharu S, et al. Single app knock-in mouse models of Alzheimer's disease. *Nat Neurosci*. 2014. <https://doi.org/10.1038/nn.3697>.
45. Greenwood FC, Hunter WM, Glover JS. The Preparation of I-131-labelled human growth hormone of high specific radioactivity. *Biochem J*. 1963. <https://doi.org/10.1042/bj0890114>.
46. Loening AM, Gambhir SS. AMIDE: a free software tool for multimodality medical image analysis. *Mol Imaging*. 2003. <https://doi.org/10.1162/15353500200303133>.
47. Ma Y, Hof PR, Grant SC, Blackband SJ, Bennett R, Slate L, et al. A three-dimensional digital atlas database of the adult C57BL/6J mouse brain by magnetic resonance microscopy. *Neuroscience*. 2005. <https://doi.org/10.1016/j.neuroscience.2005.07.014>.
48. Konishi H, Kiyama H. Microglial TREM2/DAP12 signaling: A Double-Edged sword in neural diseases. *Front Cell Neurosci*. 2018. <https://doi.org/10.3389/fncel.2018.00206>.
49. Ulrich JD, Holtzman DM. TREM2 function in Alzheimer's disease and neurodegeneration. *ACS Chem Neurosci*. 2016. <https://doi.org/10.1021/acscchemneuro.5b00313>.
50. Nordengen K, Kirsebom BE, Henjum K, Selnes P, Gísladóttir B, Wettergreen M, et al. Glial activation and inflammation along the Alzheimer's disease continuum. *J Neuroinflammation*. 2019. <https://doi.org/10.1186/s12974-019-1399-2>.
51. Lessard CB, Malnik SL, Zhou Y, Ladd TB, Cruz PE, Ran Y, et al. High-affinity interactions and signal transduction between A β oligomers and TREM2. *EMBO Mol Med*. 2018. <https://doi.org/10.15252/emmm.201809027>.
52. Gustavsson T, Syvänen S, O'Callaghan P, Sehlin D. SPECT imaging of distribution and retention of a brain-penetrating bispecific amyloid- β antibody in a mouse model of Alzheimer's disease. *Transl Neurodegener*. 2020. <https://doi.org/10.1186/s40035-020-00214-1>.

Publisher's note Springer Nature remains neutral with regard to jurisdictional claims in published maps and institutional affiliations.